Photovoltaic Performance and Morphology of Polyfluorene Blends: A Combined Microscopic and Photovoltaic Investigation

A. C. Arias,[†] J. D. MacKenzie,*[,†] R. Stevenson,[†] J. J. M. Halls,[†] M. Inbasekaran,[‡] E. P. Woo,[‡] D. Richards,[†] and R. H. Friend[†]

Cavendish Laboratory, Madingley Road, Cambridge, CB3 0HE UK, and Central and New Businesses R&D, Dow Chemical Company, Midland, Michigan 48674

Received February 9, 2001; Revised Manuscript Received June 1, 2001

ABSTRACT: The interplay between phase separation in polyfluorene blends which show photoinduced charge transfer and photovoltaic performance in photodiodes has been investigated. Phase separation length scales have been varied from several microns to tens of nanometers by limiting the time allowed for solvent-enhanced self-organization through several different processing routes. Concurrent with the decrease in feature size, an increase in maximum photovoltaic efficiency of nearly 1 order of magnitude was observed in photodiodes incorporating the phase-separated blends as the active layer. The structure of the blend films was investigated using fluorescence microscopy, fluorescence scanning near-field optical microscopy, and atomic force microscopy. In some cases, a hierarchy of micron- and nanometer-scale phase separation was observed which may explain the unexpectedly high photoresponse in devices with up to micron-scale phase separation structure. This result along with in situ fluorescence microscopy studies of the transformation process highlights the complex, multistage nature of the conjugated polymer blend formation process which generally exhibits spinodal behavior.

I. Introduction

Polyfluorene- and triarylamine-based polymers are important conjugated semiconductor materials with potential for high-performance emissive and photoresponsive applications.[1] Poly(9,9-dioctyfluorene) and related copolymers have been investigated for LEDs where charge injection, transport, and stable full-spectrum emission[2−5] are some of the critical issues to be addressed in order for the realization of practical full-color displays.[6−8] Triarylamine-based hole transport layers have shown promise for small-molecule-based LEDs,[9] and triarylamine−polyfluorene copolymers have exhibited time-of-flight hole mobilities of order 10^{-4} cm^2 V^{-1} s^{-1} at a field of 2.5×10^5 V cm^{-1}.[10]

Berggren and co-workers have shown that, by blending polymers with different emission and charge-transport characteristics, LEDs in which the emission color varies as a function of the applied voltage can be made.[11] This phenomenon arises from phase separation of the constituent polymers giving rise to domains with differing compositions and emission characteristics. Also, efficient photodiodes have been fabricated from mixtures of electron-accepting and hole-accepting polymers.[12,13] In both the LEDs and the photodiodes, the morphology of the blend film was a critical factor for device performance. It has been suggested that control of the phase separation in polymer blends could lead to cost-effective, efficient, large-area photodiodes and full color displays.[11−13]

Absorption of light in organic semiconductors creates electron−hole pairs, or excitons, which are bound at room temperature. The binding energy of an exciton in a conjugated polymer is typically on the order of 0.5 eV.[14,15] In general, the built-in potential in an organic photodiode, which results from the difference in the work function of the cathode and anode metals, is insufficient to induce charge separation. Therefore, to obtain free charges in a conjugated polymer, an effective exciton dissociation mechanism is required. It has been shown that exciton dissociation can be efficient at interfaces between certain materials with different ionization potentials and electron affinities. In this process, the electron is transferred to the material with higher electron affinity and the hole to the material with lower ionization potential.[16]

In this work, phase-separated blends of polyfluorenes were investigated and applied to photovoltaic devices. It is anticipated that the stability and transport properties of the polyfluorenes will lead to improved polymer blend photovoltaics. The chemical structures of the polyfluorene-based polymers studied here are shown in Figure 1a, where they are identified by their abbreviated names: F8BT [poly(9,9′-dioctylfluorene-*co*-benzothiadiazole)] and PFB [poly(9,9′-dioctylfluorene-*co*-bis-*N*,*N*′-(4-butylphenyl)-bis-*N*,*N*′-phenyl-1,4-phenylenediamine)]. Photoluminescence experiments show that efficient photoinduced charge transfer occurs between F8BT and PFB. F8BT is a highly luminescent polymer[8] with a high electron affinity (3.53 eV), and PFB is a high-mobility, triarylamine-based, hole transport polymer.[10]

Recently, it has been demonstrated how the efficiency of a polymer blend photovoltaic cell can be enhanced by heating the substrate to increase the evaporation rate of the solvent.[17] Through the expanded set of experiments presented here, controlling the effective length of the self-organization time period has appeared as the dominant factor affecting the photovoltaic response in these polyfluorene blends. Interestingly, high photovoltaic efficiencies relative to homopolymer devices were observed over the whole length scale range. As expected, assuming an exciton diffusion range of tens of nanometers,[18] the highest efficiencies were observed for devices with nanoscale phase separation. The persistently high efficiencies for films possessing an apparently larger-

[†] Cavendish Laboratory.
[‡] Dow Chemical Company.

10.1021/ma010240e CCC: $20.00
Published on Web 07/13/2001

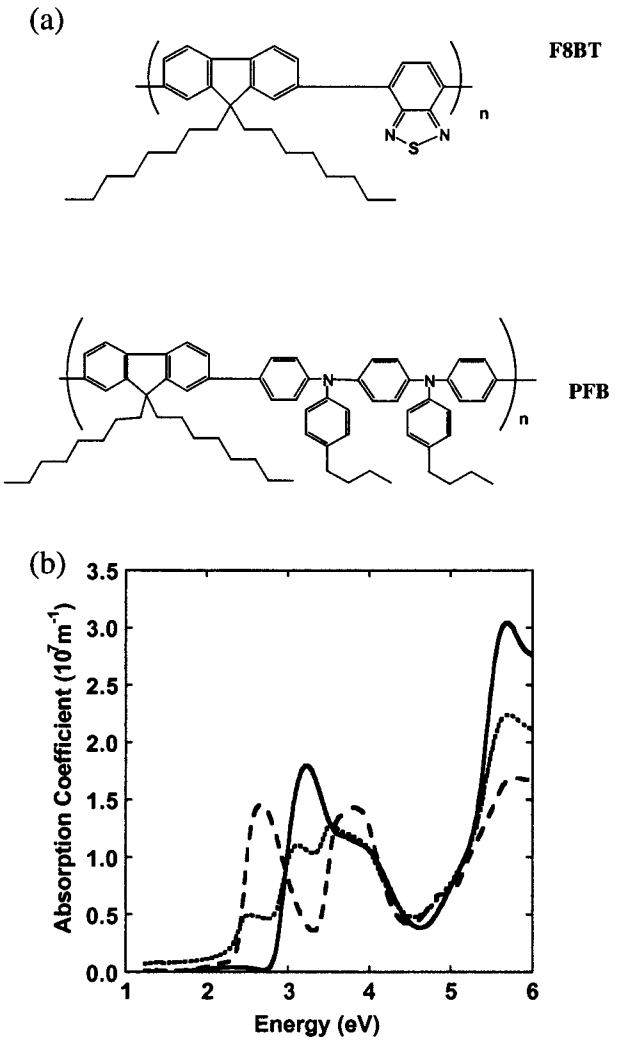

Figure 1. (a) Chemical structures of F8BT and PFB. (b) Absorption spectra of thin films (100 nm) of F8BT (dashed line), PFB (solid line), and a PFB:F8BT blend (1:1 by weight) (dotted line). The films were prepared by spin-coating from xylene solution onto quartz substrates.

scale self-organization may be explained by the presence of a concurrent nanoscale phase separation. Throughout the experimental work, fluorescence microscopy, tapping mode atomic force microscopy (AFM), and fluorescence scanning near-field optical microscopy (SNOM) have been utilized to investigate the blend structure. Issues concerning the unambiguous identification of compositionally different phases and general comparisons of the different microscopy techniques are addressed.

II. Experimental Details

Polymer solutions were prepared by dissolving the homopolymers (F8BT and PFB) separately in xylene or chloroform at a concentration of 14 mg/mL. Blends of PFB:F8BT were prepared by mixing equal quantities of each polymer solution, such that the ratio of PFB to F8BT was 1:1 by weight. Concentration dependence investigations conducted by the authors have shown that a 1:1 blend produces the highest photovoltaic external quantum efficiency (EQE) [electrons collected per incident photon]. In this work, three different procedures were used to produce thin films: (i) spin-coating films at room temperature, (ii) drop-casting films under a controlled atmosphere, and (iii) spin-coating films onto a heated substrate. Thin films for ultraviolet−visible (UV−vis) absorption spectroscopy and photoluminescence (PL) efficiency measurements were prepared, using the procedures described above, on quartz substrates. PL efficiency measurements were performed in an integrating sphere coupled to an Oriel InstaSpec IV spectrograph using the 325 nm line from a HeCd laser as the excitation source.[19]

Table 1. PL Efficiency of F8BT, PFB, and Blends Using Different Solvents and Different Treatments

material	film preparation prodedure[a]	solvent	PL efficiency/%
F8BT	SC	xylene	48.3
F8BT	SC	chloroform	57.7
PFB	SC	xylene	12.5
PFB	SC	chloroform	34.6
PFB:F8BT	SC	xylene	16.7
PFB:F8BT	SC	chloroform	3.7
PFB:F8BT	DC	chloroform	18.2
PFB:F8BT	SCH	xylene	14.2

[a] Treatments: SC = spin-coating the solution at room temperature; DC = drop-casting the solution in a controlled atmosphere; SCH = spin-coating the solution on a heated substrate.

Tapping-mode AFM was carried out using a NanoScope IIIa Dimension 3100 (Digital Instruments Inc., Santa Barbara, CA). Fluorescence microscopy images (Vickers Photoplan M41) were obtained using a Hg illumination source with a pass filter transmitting plasma lines at 365, 405, and 435 nm. Fluorescence from the sample was analyzed with a 505 nm low-pass filter. Fluorescence SNOM was carried out using the experimental configuration described by Stevenson et al.[20] The sample was illuminated in the near-field through the tip of the fiber with 488 nm excitation, and the scattered light was collected in the far field using a 0.25 N.A. microscope objective. Tip−sample distance was regulated with feedback control of the shear-force tip−sample interaction. For comparison of the fluorescence and topographical morphology of the PFB:F8BT blends, the light was collected from the sample during the SNOM measurement and was analyzed with a 520 nm bandpass filter with a 10 nm pass width. The light signal was then amplified with a photomultiplier tube using photon counting, and the resulting signal, correlated with the in-plane raster, formed the fluorescence image.

Photovoltaic devices were prepared by depositing the polymer blend film onto ITO-coated glass, using the three procedures explained above. Prior to polymer deposition, the substrates were cleaned in an ultrasonic bath with acetone and 2-propanol and subsequently treated in an oxygen-plasma etcher. It has been shown that this treatment reduces the surface roughness of ITO and increases its work function.[21] Aluminum contacts, 150 nm thick, were deposited by thermal evaporation onto the polymer film. The active area of each pixel, defined by the overlap of the aluminum contacts with the patterned ITO, was 1 mm^2. The devices were fabricated in a nitrogen-filled glovebox, unless otherwise specified.

The diodes were electrically characterized under a vacuum of order 10^{-7} mbar. For determination of the spectral response of the photocurrent, a Xe arc lamp, spectrally resolved by a monochromator, illuminated the diodes from the ITO side, at an intensity of order 0.1 mW cm^{-2} at each wavelength interval. The spectral dependence of the power incident on the devices was calibrated with a Si photodiode reference.

III. Results

The UV−vis absorption spectra of thin, spin-cast films of PFB, F8BT, and the PFB:F8BT blend are shown in Figure 1b. The absorption spectra of the blends follows the linear superposition of the spectrum of the individual polymers, indicating that significant ground-state charge transfer does not occur in these blends. The PL efficiencies of the individual polymers and the blend were also measured, and the results are summarized in Table 1.

The 50 μm × 50 μm AFM surface morphologies of films prepared by spin-coating the blend from xylene

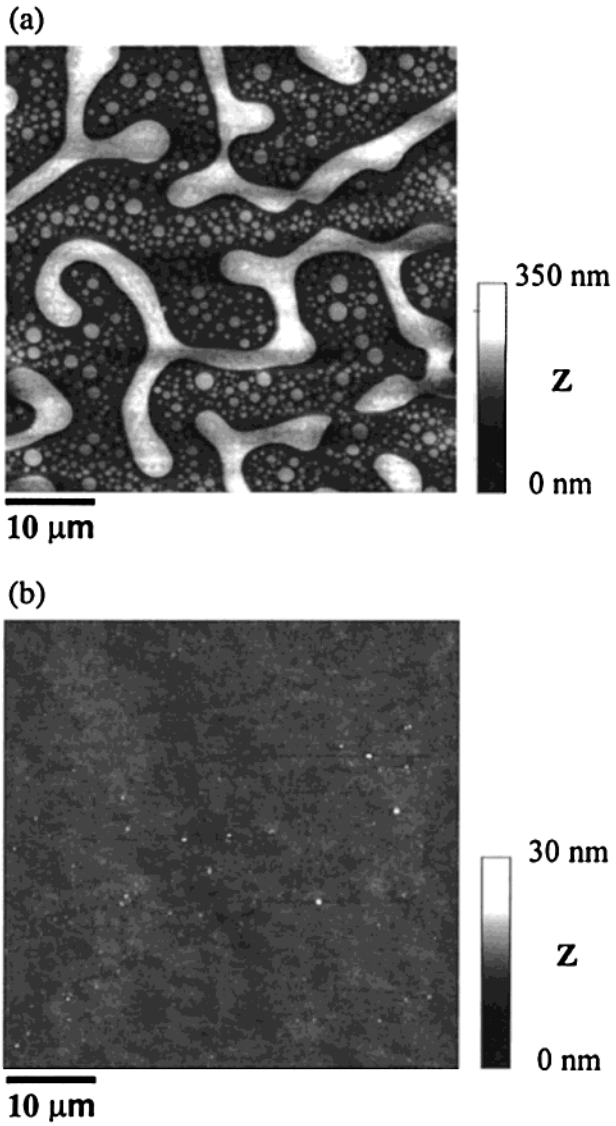

Figure 2. (a) Topographical AFM image of a spun PFB:F8BT film, using xylene as the solvent. (b) Topographical AFM image of a spun PFB:F8BT film, using chloroform as the solvent.

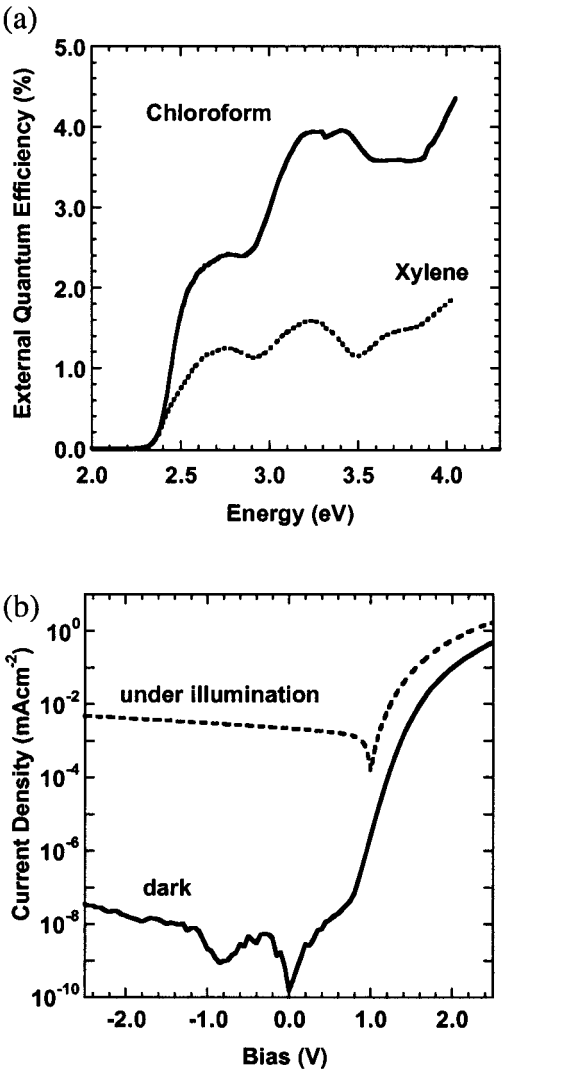

Figure 3. (a) Short-circuit EQE action spectra of photovoltaic devices fabricated by spin-coating from 1:1 blend by weight of PFB:F8BT from a chloroform solution (solid line) and from a xylene solution (dotted line). (b) The current−voltage characteristics of an ITO/PFB:F8BT (200 nm, spun)/Al device, in the dark (solid line) and under illumination at wavelength of 466 nm [2.66 eV] (dashed line). The rectification ratio at ±3 V, measured in the dark, is 1.4×10^7.

and chloroform solutions are shown in parts a and b of Figure 2, respectively. The scale of the phase separation of films prepared from a chloroform solution is much finer (less than 100 nm) than the phase separation of films prepared by spin-coating the blend from a xylene solution. In addition, PFB:F8BT films prepared by spin-coating from a chloroform solution show charge separation quenching of the photoluminescence to a level of 3.7%, as shown in Table 1. Photovoltaic devices made in this way show an EQE of 4% for 3.2 eV excitation whereas devices made by spin-coating the xylene solution show an EQE of 1.8%. Figure 3a illustrates the spectral dependence of the short-circuit photocurrent for devices made from chloroform and xylene solutions. The photocurrent action spectra have been corrected for the absorption spectrum of the ITO-coated glass substrate. Current−voltage characteristics of the blend photodiodes are shown in Figure 3b; the rectification ratio is 10^7 at ± 3 V, and the fill factor is 0.48 under illumination at 466 nm.

The chloroform blend solutions were diluted to a polymer concentration of 1.75 mg mL^{-1} to prepare films by drop-casting. The drop-casting period was extended by placing the sample inside a sealed chamber in which a high concentration of solvent vapor was maintained. An AFM image of films prepared with this procedure is shown in Figure 4a. The EQE at 3.2 eV for devices fabricated from drop-cast films was ∼2.0%. The photocurrent action spectra of photovoltaic devices made from chloroform solutions, with low (drop-casting) and high (spin-coating) evaporation rates of chloroform, are compared in Figure 4b.

Figure 5a shows a AFM image of a PFB:F8BT film spin-coated from a xylene solution onto a heated substrate. The spin-coater chuck and the substrate were heated to 40 °C with a high-intensity halogen lamp, which was extinguished immediately before spin-coating. The PL efficiency of films prepared in this way is reduced compared to films prepared at room temperature (Table 1). The photovoltaic EQE at 3.2 eV for these devices was 1.6% as compared to 0.7% for devices spun at room temperature. The photocurrent action spectra of devices spun at room temperature and at 40 °C are shown in Figure 5b.

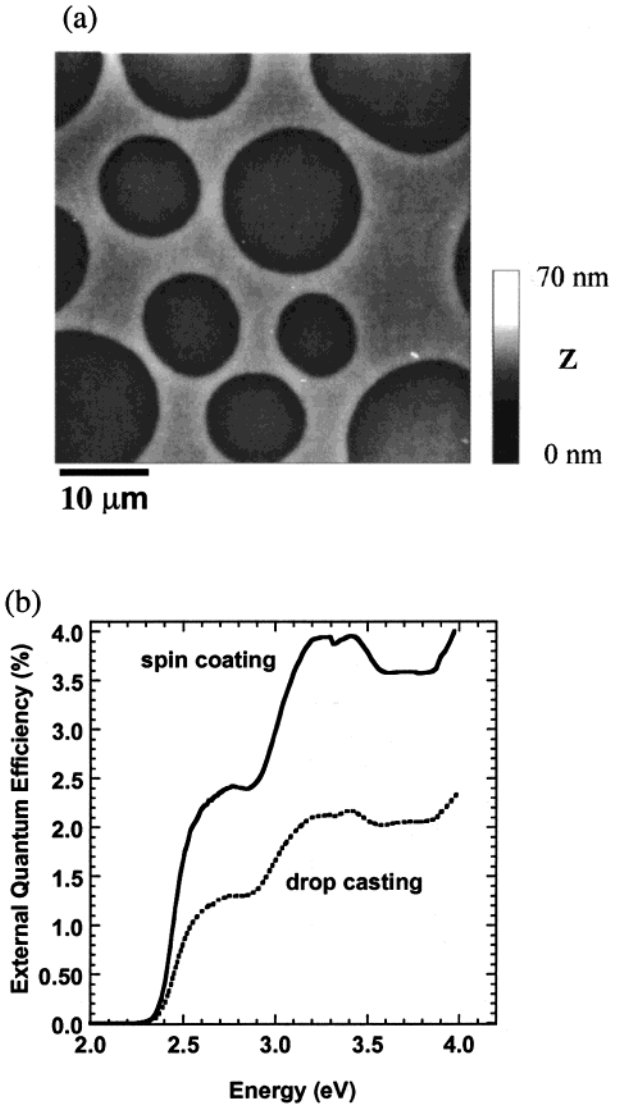

Figure 4. (a) Topographical AFM image of the PFB:F8BT blend film prepared by drop-casting the chloroform solution under a solvent-saturated atmosphere. (b) Short-circuit EQE action spectra of PFB:F8BT blend photovoltaic devices fabricated by spin-coating the chloroform solution (high evaporation rate, solid line) and by drop-casting the chloroform solution (low evaporation rate, dotted line).

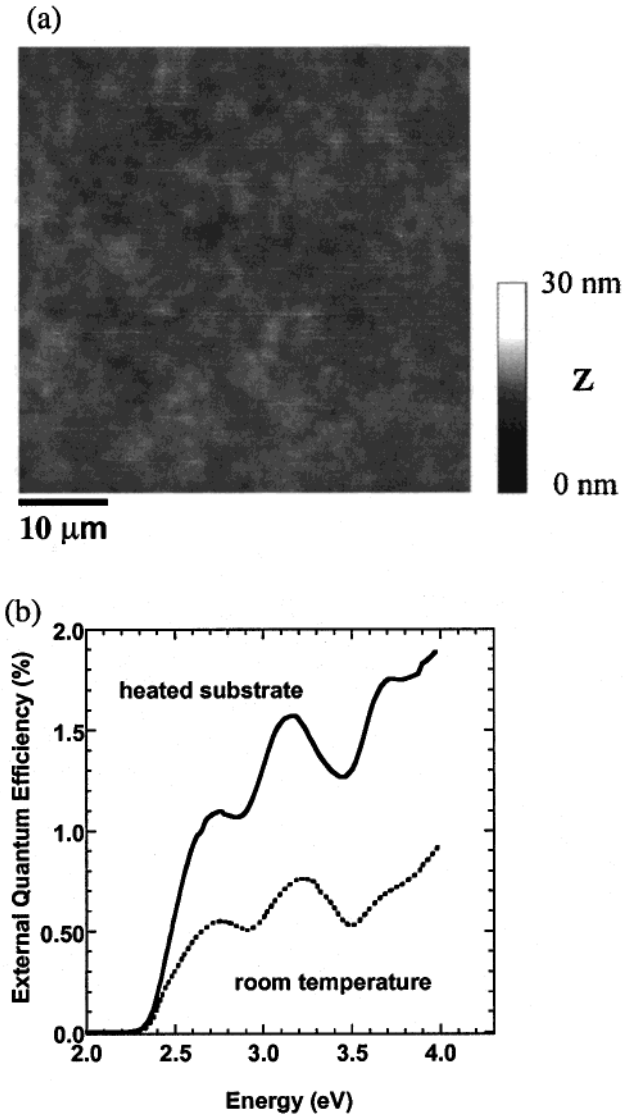

Figure 5. (a) Topographical AFM image of the PFB:F8BT blend film prepared by spin-coating the xylene solution on top of a heated substrate (40 °C). (b) Short-circuit EQE action spectra of PFB:F8BT blend photovoltaic devices fabricated by spin-coating the xylene solution at room temperature (dotted line) and by spin-coating the xylene solution onto a heated substrate (40 °C, solid line).

An in-situ fluorescence microscopy experiment was conducted to further elucidate the nature of the phase separation mechanism. Figure 6a−d shows successive fluorescence images taken from a PFB:F8BT sample as it was being transformed to a thin film during drop-casting from a xylene solution. The total time for the depicted transformation was approximately 5 s.

Figure 7a is a topographical SNOM image of a polymer blend film made by spin-coating from a xylene solution. The image was produced by rastering the SNOM tip in the plane of the sample and recording the tip displacement which is regulated through feedback of a constant shear force interaction of the oscillating tip with the sample surface. The topography imaged with this configuration follows that observed for AFM of similar samples. The emission spectra labeled A(n) to D(n) in Figure 7b were collected at the corresponding positions marked in the topographical image (a), with n denoting the order of the measurements. Figure 8 depicts plan-view fluorescence (a) and corresponding topography (b) images from the SNOM measurement along with a tapping mode AFM (c) image of the active layer of a PFB:F8BT blend photodiode. The fabrication and performance of this device have been described previously.[17]

Figure 9a shows 10 μm × 10 μm tapping mode AFM images of a film spin-coated from xylene solution. The left half of the figure shows the height image while the phase response image is shown on the right. Figure 9b shows 500 nm × 500 nm height and phase AFM images of the vicinity of the sample surface marked by a white square in Figure 9a.

IV. Discussion

Miscibility between polymers is determined by a balance of enthalpic and entropic contributions to the free energy of mixing. The entropy of mixing is small, making the enthalpic interactions decisive for miscibility.[22] Even very small differences in polymer structure

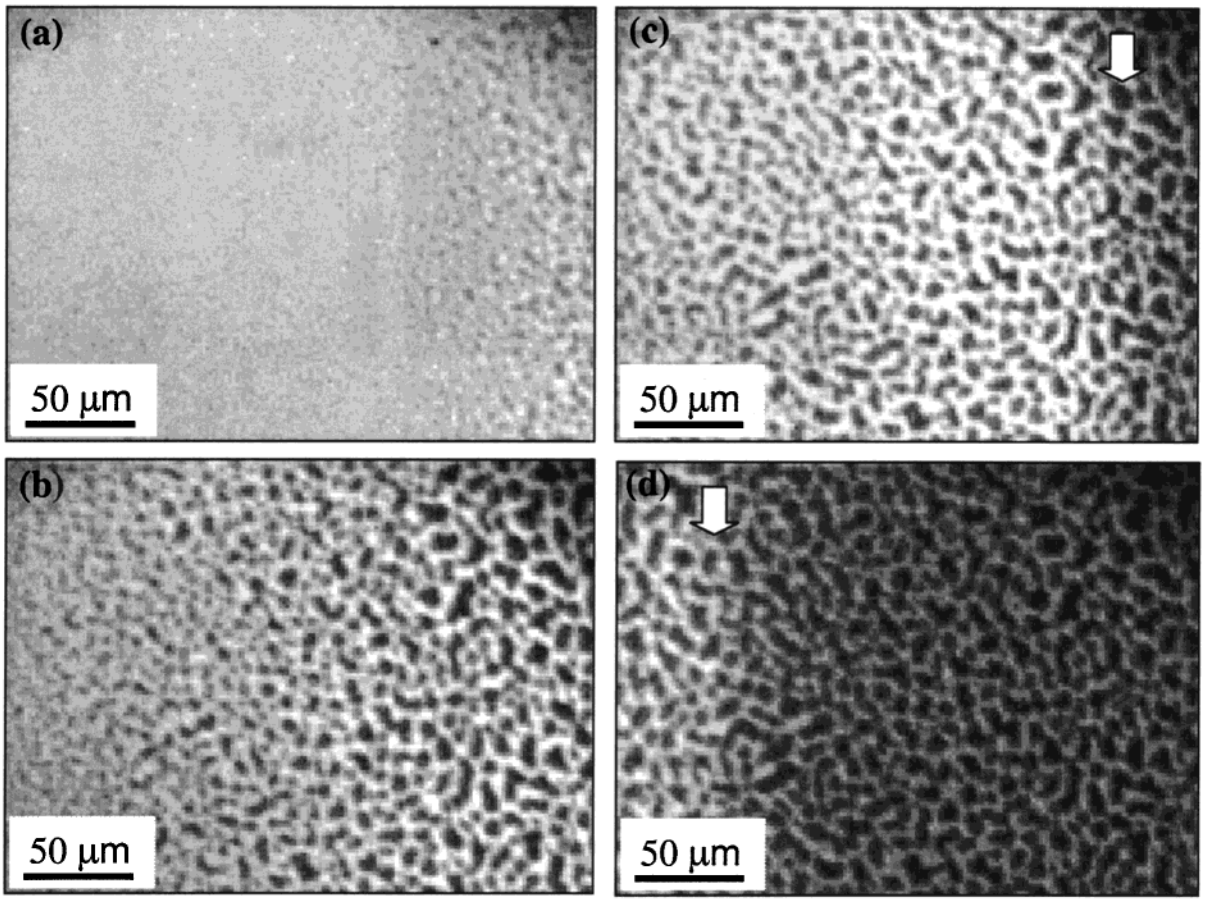

Figure 6. In-situ fluorescence images of a PFB:F8BT film during transformation from solution. The series of consecutive images show the movement of a solidification front moving from right to left. In (a) the majority of the field is still strongly fluorescing liquid solution. As the front sweeps through the field of view in successive images, coalescence and coarsening can be observed as well as a distinct final quenching front that lags behind the large-scale separation. This quenching front is marked by a white arrow in (c) and (d).

can lead to positive enthalpic effects that dominate the entropic contribution to the free energy of mixing. This drives polymers in a blend to phase separate, giving rise to self-organized blend structures on the micro- and nanoscale. It is well-known in model polymer blends that, if the diffusivity of the polymers is high enough and if given enough time, the phase separation can go through several stages of coarsening.[23,24] Also, surface interactions and film stability can be critical in the formation process.[25] Consequently, the preparation method of the blend films plays an important role in controlling the phase separation and ultimately the photovoltaic response.

Rapid solvent evaporation occurs during spin-coating blends from chloroform solution in ambient conditions. This prevents significant rearrangement of the polymer chains and quenches a fine phase separation, as in Figure 2b. In addition, the strong reduction of PL shows that excitons are very efficiently dissociated in the blend, indicating that PFB and F8BT are phase-separated on a scale similar to the exciton diffusion length, tens of nanometers. Consequently, devices fabricated from a chloroform solution demonstrated significantly higher photovoltaic EQE than those fabricated from a more slowly evaporating xylene solution (Figure 3a). In contrast, films prepared by drop-casting the blend in a chloroform-saturated atmosphere undergo a much slower transformation. As a result, these films show phase separation on a much larger scale than films prepared by spin-coating from the same solvent. The large-scale morphology of the drop-cast samples is readily apparent in the AFM topography image shown in Figure 4a. Concurrent with an increase in feature size for the drop-cast films, a 5-fold increase in PL quantum efficiency was observed. Fluorescence microscopy shows that the higher phase observed in AFM images corresponds to an F8BT-emitting phase. However, photoluminescence efficiency measurements show that even in films with apparent in-plane phase separation on a length scale of tens of microns, the PL is significantly reduced. As displayed in Table 1, the PL efficiency of a pure F8BT film is 58%, while the PL efficiency of a PFB:F8BT blend prepared by drop-casting is 18%. This cannot be accounted for by the relatively small interfacial area between the phases. This result suggests that the distinct phases observed through microscopy are not pure. When correlating the surface morphologies and the optical properties of the films and devices, it should be noted that the morphological characterization techniques employed here largely reflect the in-plane separation evident at the sample surface. There is the possibility of vertical anisotropy of the films' composition, which would likely affect the optical and electrical response of the polymer blend films. This is an interesting issue, which is relevant to blend photodiodes and LEDs, and it is currently under study.

The high PL quenching, and therefore the high probability of exciton dissociation in the spin-coated

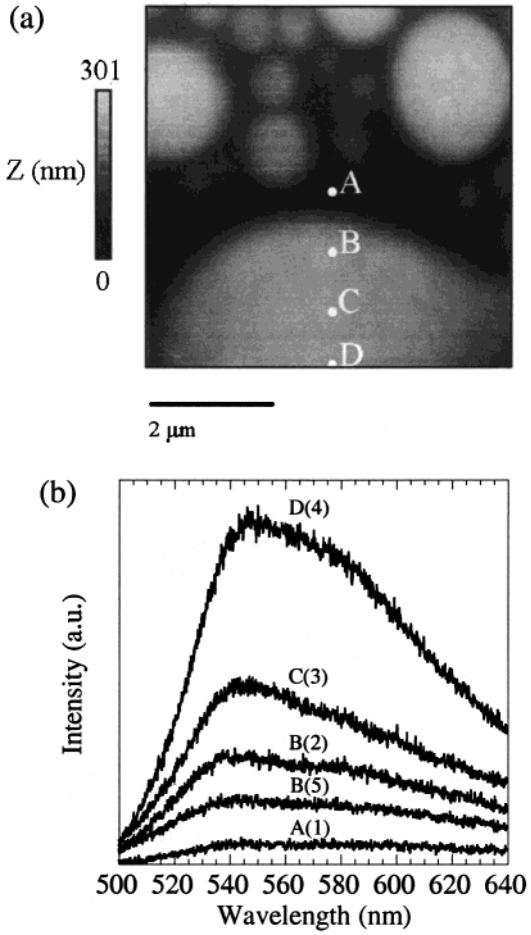

Figure 7. (a) Shear-force topographical image of a polyfluorene blend. (b) Emission spectra (A−D) taken with the SNOM at the corresponding positions marked in the topographical image.

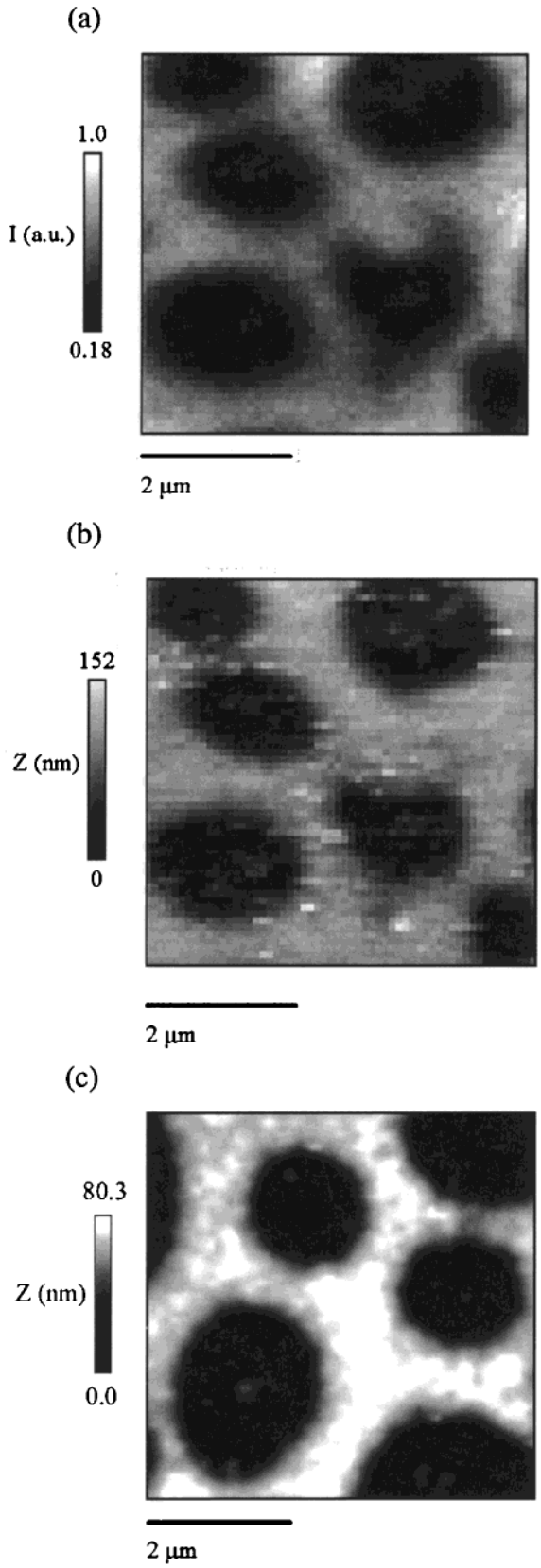

Figure 8. (a) Fluorescence SNOM, (b) shear-force topography, and (c) AFM topography images of a PFB:F8BT blend. Note (a) and (b) are of the same area measured simultaneously.

films from chloroform, explains the higher photovoltaic efficiencies observed for these devices. However, the maximum EQE for the spin-coated devices was greater than that of the drop-cast devices by only a factor of 2. This weaker dependence of the photovoltaic efficiency on feature size compared to the dependence of the PL quenching, along with the AFM and fluorescence microscopy, suggests that a tradeoff exists between optimized charge separation and transport in these samples. In the case of the fine phase separation in the spin-coated samples, efficient exciton dissociation occurs while transport of the charge to the contacts may be somewhat restricted. In the drop-cast samples, the apparent columnar structure, with a domain size on the order of tens of microns, provides for efficient charge transport from the limited amount of PFB/F8BT interface. In addition to these effects, equilibrium, solubility, or kinetically induced metastability of F8BT in the predominately PFB regions of the drop-cast sample, as well as photonic effects, may need to be considered. The PL results discussed previously and initial investigations done with blends composed of different PFB:F8BT ratios suggest that the F8BT used in this work is less soluble in PFB than PFB in F8BT.

Phase separation in PFB:F8BT films has also been manipulated by dissolving the polymers in different solvents, such as chloroform and xylene. The vapor pressure of chloroform is 160 mmHg at 20 °C, whereas the vapor pressure of xylene is only 6.72 mmHg at 21 °C.[26] Since chloroform evaporates much faster than xylene, it was expected that films prepared from a chloroform solution would exhibit phase separation on a smaller scale than films prepared from a xylene

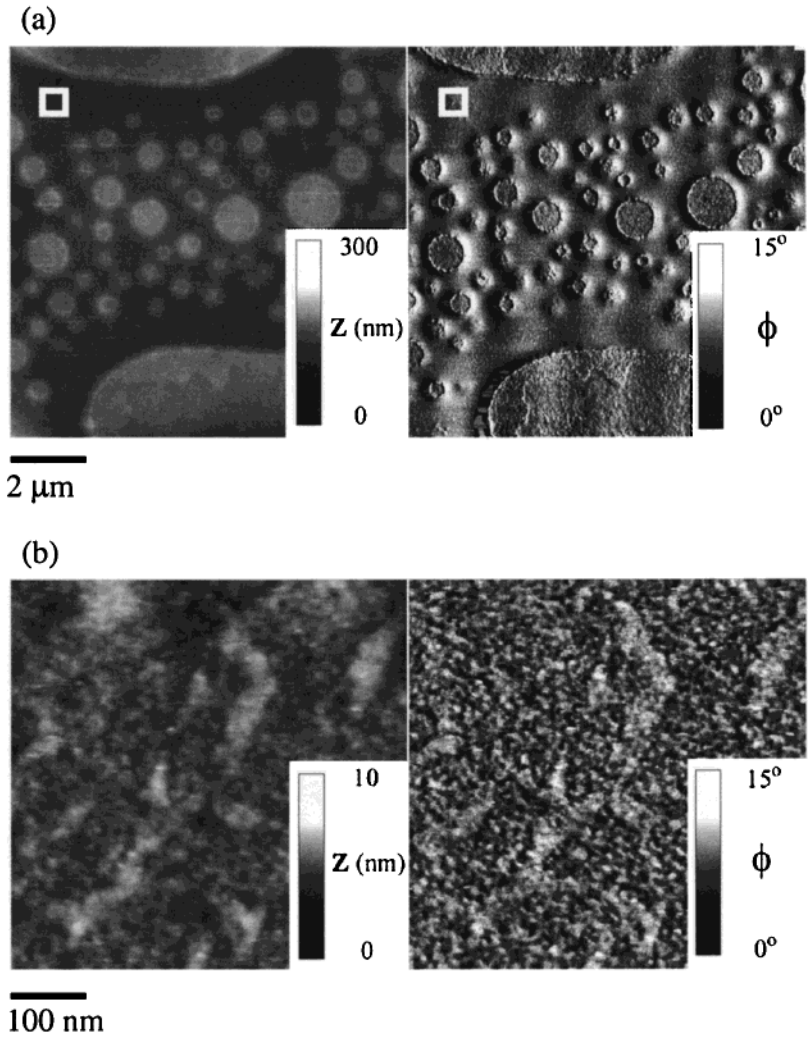

Figure 9. AFM images of PFB;F8BT film spin-coated from xylene solution. The left half of the figures shows the height images and the phase response images are shown on the right: (a) 10 μm × 10 μm and (b) 500 nm × 500 nm which was taken in the vicinity of the sample marked by the white square in (a).

solution. Indeed, it was observed that the phase separation, apparent in the fluorescence microscopy, of films prepared by spin-coating the blend from xylene falls in the micrometer range and resembles model structures of a relatively advanced stage of spinodal decomposition. Increasing the evaporation rate of xylene, by means of heating the substrate before spin-coating, quenched the phase separation to the nanometer scale and increased the photovoltaic efficiency (Figure 5). The change in the phase separation scale can be seen by comparing the morphology of the heated sample, shown in Figure 5a, with the unheated morphology depicted in Figure 2a. The photovoltaic efficiencies of the devices made from xylene on heated substrates were higher than that of the xylene samples processed in ambient conditions and were similar to the chloroform/ambient atmosphere devices. Therefore, the evaporation rate and not the chemical structure of the solvent was the critical parameter.

Clearly, knowledge of the morphology and compositional microstructure is critical to the understanding and development of photoresponsive polymer blend films. However, thin films of conjugated polymer blends present a unique challenge as they fall at the limits of many of the well-developed characterization tools developed primarily for metals and inorganic semiconductors. A significant part of this study has been the utilization and cross-comparison of morphological characterization techniques. Conventional fluorescence microscopy, AFM, and fluorescence SNOM have all been combined to identify and analyze the separated phases in PFB:F8BT blends on length scales ranging from tens of microns to nanometers. As well, higher resolution AFM of PFB:F8BT films suggests that there may be a hierarchy of microstructures on micro- and nanoscales in films prepared under certain conditions. In this report, AFM imaging has been drawn on extensively to correlate the processing parameters, photovoltaic properties, and microstructure. Although they can suggest a well-defined phase separation, AFM topographical features by themselves do not give an unambiguous picture of the phase composition. Here, optical fluorescence techniques have been used to associate structural features more clearly with composition.

The solidification of PFB:F8BT films during solvent casting was studied in some detail with in-situ fluorescence microscopy. In these experiments, the formation of films was recorded in real time from PFB:F8BT xylene solution drop-cast on glass. The series of consecutive images in Figure 6 show the movement of a solidification front from right to left across the field of view of the microscope. As in all other fluorescence

microscopy presented in this paper, the bright signal here represents filtered F8BT emission. In Figure 6a the majority of the field of view is still strongly fluorescing liquid solution. As the front sweeps across the film in (b) through (d), liquid coalescence, coarsening, and immobilization can be observed. Following the large-scale separation that occurs during the initial solidification, a distinct, final luminescence quench front sweeps across the film. This quenching front is marked by a white arrow in (c) and (d). This front may represent the collapse of the solidified (in the context of large-scale flow processes) but still solvent-swollen film as the last of the xylene leaves the film. During this step, intermolecular interaction increases as the remaining solvent leaves, leading to the onset of charge transfer and luminescence quenching between PFB and F8BT. This multistage behavior is likely a result of the complex competition between the enthalpic driving forces separating the polymer, dewetting forces, the evolving solubilities, and the slowing molecular mobility as solvent leaves the film.

Fluorescence SNOM and conventional fluorescence microscopy were used to study the blend structure and to validate the interpretation of the AFM results. Using 488 nm (2.54 eV) excitation, F8BT is selectively excited as it has the lower energy absorption edge of the two components of the blend. By analyzing the emitted light from the blend at localized positions and comparing this to the topographical image produced by the SNOM, a strong correlation between the raised topographical features and the presence of F8BT emission was seen, as depicted in Figure 7. The decrease in collected fluorescence intensity between measurements B(2) and B(5) is likely to be due to local photobleaching of the sample.[27,28] There is clearly good agreement between the fluorescence and shear-force topographical maps showing localization of fluorescent F8BT-rich regions in a raised, continuous, micron-scale network (Figure 8a,b). The SNOM technique, as it is employed here, is surface sensitive, as compared to conventional fluorescence microscopy. On the basis of previous modeling,[29] the skin depth is assumed to be in the range 20−30 nm for the polymers used in this work. The height image from the tapping-mode AFM scan of the same region of the sample exhibits a very similar morphology and shows that the F8BT-rich network is raised and distinctly textured with respect to the other phase (Figure 8c). This correlation between the SNOM and AFM results indicates the utility of AFM for studying these blends where time and resolution constraints may limit the use of SNOM.

One interesting issue, highlighted by the device studies, is the relationship between phase separation and device efficiency. Consistently, an increase of external quantum efficiency of only a factor of 2−3 has been observed for series of samples where the length scale of the phase separation appears to vary over orders of magnitude. A stronger relationship between efficiency and phase separation is expected if the efficiency of the photovoltaic effect is limited by the availability of a heteropolymer interface within an exciton diffusion length from the site of photon absorption. For a columnar, segregated, or true 3-D interpenetrating network structure in the blend film, a linear or superlinear dependence of efficiency on length scale might be expected. Higher resolution topographic and phase AFM images of some PFB:F8BT films indicate that there may be a hierarchy of phase separations present. AFM phase imaging has been used previously in the investigation of polymer photovoltaic thin films.[30]

The 10 μm × 10 μm AFM images of the PFB:F8BT films spun from xylene solution shown in Figure 9a are dominated by a large, abrupt, micron-scale phase separation. The elongated and the smaller circular surface features likely developed at different times during the evaporation process in a manner similar to that observed by Thiele et al.[31] where multiple scales of dewetting features were attributed to heterogeneous nucleation and an evolving spinodal instability scale. It should be noted that in this work little difference in the scale of the phase separation was seen for films transformed on glass and quartz surfaces with different cleaning and preparation histories. Fluorescence microscopy of the same film correlated these micron-scale features with a strong compositional separation of the PFB and F8BT. However, closer analysis of the PFB-rich regions shows a subtexture, as shown in Figure 9b. In both images, there appears to be a distinct morphology composed of a semicontinuous minority network phase, with a typical feature width of 20−40 nm. A similar morphology was consistently observed at several points within the micron-scale PFB-rich regions. AFM images of pure PFB films at this magnification more closely resembled the background textures seen in Figure 9b. It should be noted that these nanoscale structures, although of the same length scale, are qualitatively different than the fine structure observed for the highest efficiency, most rapidly formed PFB:F8BT devices of this study and in prior work.[17] Although there may be other factors affecting photovoltaic EQE of PFB:F8BT thin film photodiodes such as percolation continuity and vertical segregation, these AFM results suggest that comparatively high efficiencies for PFB:F8BT devices with large-scale phase separation maybe be due to the presence of a finer scale of self-organization. The complex structures observed in these samples are likely due to the evolving, nonequilibrium nature of the transformation process in which molecular mobility is decreasing with solvent evaporation as the solubility limits are approached. At the same time film stability, in terms of dewetting, is evolving as the thickness and the composition of the solvent + blend film changes.

It has been demonstrated in this work that, by controlling the kinetics of the film formation process, different stages in the evolution of the phase separation can be frozen in. In general, the phase separation structures observed for PFB:F8BT thin films in this study and previously[17] are consistent with a spinodal-type decomposition mechanism. Some of the characteristics and morphologies of the conjugated polymer blend films studied here follow results recently observed for nonconjugated multicomponent polymer thin films.[25,32] Under controlled conditions, at least partial activity of nearly all of the regimes of spinodal decomposition can be observed either directly or indirectly. This includes an initial fine-scale, bicontinuous separation; hydrodynamic regimes, such as in Figure 2a; and coalescence. From the surface topographies, especially in the case of intermediate transformation times, the presence of significant surface relief, and the evolution of some of those features indicates that dewetting and liquid film stability also shapes the morphology at least during some portion of the film formation process. This includes the instability of elongated raised structures, such as

those in Figure 2a, which break down under longer transformation times such as spin-coating from xylene solution in a partially saturated atmosphere. Dewetting in unstable model thin-film systems is known to exhibit characteristic spinodal morphologies.[33] And, multiple-scale dewetting phenomena have been studied in dynamic experiments.[31] However, the microscopical evidence for the blends in this work, further discussed below, suggests that in all cases a significant compositional phase separation is nearly always present in the spinodal morphologies.

V. Conclusions

Limiting the phase separation kinetics through solvent evaporation control can be used to improve and understand the structure and performance of polyfluorene photovoltaic blends. By varying the solvent, the substrate temperature, and the saturation of the atmosphere over the transforming film, the characteristic phase separation length scales could be varied from tens of nanometers or less up to tens of microns. It was found that the quenching-in of a nanoscale phase separation structure, independent of the chemical nature of the solvent, leads to a high photovoltaic efficiency. Photovoltaic efficiencies varying from 0.5% to 4% were obtained. To study the photovoltaic efficiency−morphology relationship, scanning probe and light microscopies were investigated and applied. Good agreement was seen between the submicron optical structure as determined by fluorescence SNOM and the surface topography seen in tapping-mode AFM. The nanoscale capability of the AFM revealed a finer structure in some films where a more obvious micron-scale structure is also present. In situ microscopy studies of the transformation process further emphasize the complex nature of the film formation process. This may explain the weaker than expected dependence of the photovoltaic external quantum efficiency on the apparent phase separation size. This multilevel organization also suggests the possibility for polymer blends engineered at several length scales to optimize, for example, charge separation and transport to the contacts.

Acknowledgment. A.C.A. thanks the Brazillian government for funding under a CNPq scholarship and Dr. Henning Sirringhaus for valuable discussions. This work has been partially supported by the European Commission under Brite-Euram Contract BRPR-CT97-0469. We gratefully acknowledge the assistance of Cambridge Display Technology Ltd. in the provision of AFM equipment.

References and Notes

(1) Friend, R. H.; Gymer, R. W.; Holmes, A. B.; Burroughes, J. H.; Marks, R. N.; Taliani, C.; Bradley, D. D. C.; Santos, D. A. d.; Brédas, J. L.; Lögdlund, M.; Salaneck, W. R. *Nature* **1999**, *397*, 121.
(2) Yang, Y.; Pei, Q.; Heeger, A. J. *J. Appl. Phys.* **1996**, *79*, 934.
(3) Tessler, N.; Harrison, N. T.; Friend, R. H. *Adv. Mater.* **1998**, *10*, 64.
(4) Kim, J. S.; Friend, R. H.; Cacialli, F. *Appl. Phys. Lett.* **1999**, *74*, 3084.
(5) Ho, P. K. H.; Kim, J. S.; Burroughes, J. H.; Becker, H.; Li, S. F. Y.; Brown, T. M.; Cacialli, F.; Friend, R. H. *Nature* **2000**, *404*, 481.
(6) Klaerner, G.; Miller, R. D. *Macromolecules* **1998**, *31*, 2007.
(7) Grice, A. W.; Bradley, D. D. C.; Bernius, M. T.; Inbasekaran, M.; Wu, W. W.; Woo, E. P. *Appl. Phys. Lett.* **1998**, *73*, 629.
(8) He, Y.; Gong, S.; Hattori, R.; Kanicki, J. *Appl. Phys. Lett.* **1999**, *74*, 2265.
(9) Tang, C. W.; Slyke, S. A. V. *Appl. Phys. Lett.* **1987**, *51*, 913.
(10) Redecker, M.; Bradley, D. D. C.; Inbasekaran, M.; Wu, W. W.; Woo, E. P. *Adv. Mater.* **1999**, *11*, 241.
(11) Berggren, M.; Inganäs, O.; Gustafsson, G.; Rasmusson, J.; Anderson, M. R.; Hjertberg, T.; Wennerström, O. *Nature* **1994**, *372*, 444.
(12) Halls, J. J. M.; Walsh, C. A.; Greenham, N. C.; Marseglia, E. A.; Friend, R. H.; Moratti, S. C.; Holmes, A. B. *Nature* **1995**, *376*, 498.
(13) Yu, G.; Heeger, A. J. *J. Appl. Phys.* **1995**, *78*, 4510.
(14) Marks, R. N.; Halls, J. J. M.; Bradley, D. D. C.; Friend, R. H.; Holmes, A. B. *J. Phys.: Condens. Matter* **1994**, *6*, 1379.
(15) Brédas, J.; Cornil, J.; Heeger, A. J. *Adv. Mater.* **1996**, *8*, 447.
(16) Tang, C. W. *J. Appl. Phys.* **1986**, *48*, 183.
(17) Halls, J. J. M.; Arias, A. C.; MacKenzie, J. D.; Inbasekaran, M.; Woo, E. P.; Friend, R. H. *Adv. Mater.* **2000**, *12*, 498.
(18) Halls, J. J. M.; Pichler, K.; Friend, R. H.; Moratti, S. C.; Holmes, A. B. *Appl. Phys. Lett.* **1996**, *68*, 3120.
(19) de Mello, J. C.; Wittmann, H. F.; Friend, R. H. *Adv. Mater.* **1997**, *9*, 230.
(20) Stevenson, R.; Granström, M.; Richards, D. *Appl. Phys. Lett.* **1999**, *75*, 1574.
(21) Kim, J. S.; Granström, M.; Friend, R. H.; Johansson, N.; Salaneck, W. R.; Daik, R.; Feast, W. J.; Cacialli, F. C. *J. Appl. Phys.* **1998**, *84*, 6859.
(22) Folkes, M. J.; Hope, P. S. *Polymer Blends and Alloys*, 1st ed.; Blackie Academic & Professional: London, 1993.
(23) Utracki, L. A. *Polymer Alloys and Blends: Thermodynamics and Rheology*; Hanser: New York, 1989.
(24) Sperling, L. H. *Introduction to Physical Polymer Science*, 2nd ed.; John Wiley & Sons: New York, 1992.
(25) Böltau, M.; Walhein, S.; Mlynek, J.; Krausch, G.; Steiner, U. *Nature* **1998**, *391*, 877.
(26) Weast, R. C.; Lide, D. R. *CRC Handbook of Chemistry Physics*, 70th ed.; CRC Press: Boca Raton, FL, 1990.
(27) Jong, M. J. M. D.; Vissenberg, M. C. J. M. *Philips J. Res.* **1998**, *51*, 495.
(28) Papadimitrakopoulos, F.; Konstadinidis, K.; Miller, T. M.; Opila, R.; Chandross, E. A.; Galvin, M. E. *Chem. Mater.* **1994**, *6*, 1563.
(29) Stevenson, R.; Richards, D. *Semicond. Sci. Technol.* **1998**, *13*, 882.
(30) Granström, M.; Petritsch, K.; Arias, A. C.; Lux, A.; Andersson, M. R.; Friend, R. H. *Nature* **1998**, *395*, 257.
(31) Thiele, U.; Mertig, M.; Pompe, W. *Phys. Rev. Lett.* **1998**, *80*, 2869.
(32) Walhein, S.; Schäffer, E.; Mlynek, J.; Steiner, U. *Science* **1999**, *283*, 520.
(33) Sharma, A.; Khanna, R. *Phys. Rev. Lett.* **1998**, *81*, 3463.

MA010240E